Development, Modeling and Control of a Dual Tilt-Wing UAV in Vertical Flight

Luz-Maria Sanchez-Rivera, Rogelio Lozano, Alfredo Arias

Noname manuscript No.
(will be inserted by the editor)

Development, modeling and control of a Dual Tilt-Wing UAV in vertical flight

Luz M. Sanchez-Rivera* · **Rogelio Lozano** · **Alfredo Arias-Montano**

Received: date / Accepted: date

Abstract Hybrid Unmanned Aerial Vehicles (H-UAVs) are currently a very interesting field of research in the modern scientific community due to their ability to perform Vertical Take-Off and Landing (VTOL) and Conventional Take-Off and Landing (CTOL). This paper focuses on the Tilt-wing UAV, a vehicle capable to performing both flight modes (VTOL and CTOL). Hovering and vertical flight, which is characteristic of helicopters, and high cruising speeds, which are a characteristic of fixed-wing are achieved by a tilt-wing mechanism enabling to modify the rotor's thrust direction [1]. The UAV complete dynamic model is obtained using the Newton-Euler formulation, it includes aerodynamic effects, as the drag and lift forces of the wings which are a function of airstream generated by the rotors, the cruise speed, tilt-wing angle and angle of attack, furthermore, additional aerodynamic effects caused by the empennage are considered [2]. The airstream velocity generated by the rotors is studied in a test bench. The projected area on the UAV wing that is affected by the airstream generated by the rotors is specified and 3D aerodynamic analysis is performed for this region. In addition, aerodynamic coefficients of the UAV in VTOL mode are calculated by using Computational Fluid Dynamics method (CFD) and are embedded into the nonlinear dynamic model. To validate the complete dynamic model, PD controllers are designed for altitude and attitude control of the vehicle in VTOL mode, the controllers are simulated and implemented in the vehicle for indoor and outdoor flight experiments.

This work was supported by CONACyT, UMI-LAFMIA 3175 CNRS and CINVESTAV-IPN.

Luz M. Sanchez-Rivera
Laboratoire Franco-Mexicain d' Informatique et Automatique, UMI LAFMIA 3175 CNRS-CINVESTAV
Av. IPN 2508, San Pedro Zacatenco, 07360, Ciudad de México, México
E-mail: luz.maria.sanchez@cinvestav.mx

Rogelio Lozano
Laboratoire Heudiasyc UMR CNRS 6599, Université de Technologie de Compiègne
Centre de Recherches de Royallieu 60205, Compiègne, France
E-mail: rlozano@hds.utc.fr

Alfredo Arias-Montano
Escuela Superior de Ingeniería Mecánica y Eléctrica UP Ticomán, IPN
Av. Ticomán 600, San José Ticomán, 07340, Ciudad de México, México
E-mail: aarias@ipn.mx

Keywords Dual Tilt-wing · VTOL flight mode · Complete dynamic model · Drag and lift forces · PD

1 Introduction

In recent time, many UAV types have been developed with the purpose to expand its features, flight modes, applications, missions, etc. Actually, UAVs can be classified into three groups: fixed-wing UAVs (airplane), rotary-wing UAVs (Multi-rotor) and hybrid UAVs.

Hybrid UAV combines the capabilities of a fixed-wing (large cruising speed) and a rotary-wing (vertical take-off and landing) by means of its three flight modes: VTOL, transition and CTOL. Based on whether or not the fuselage tilts, hybrid UAV can be further divided into two categories: convertiplane and tailsitter. Tilt-rotor and tilt-wing are some examples of convertiplanes, both vehicles can perform the transition between VTOL and CTOL flight modes by means of a tilt mechanism that changes the angle of the rotors or the wings with rotors.

In the area of tilt rotors there has been more progress and focus in the last years [3], [4], [5], vehicles with four, three and two rotors in addition to main rotor have been a source of research for its different flight modes, from the control design to experimental flight tests. On the other hand, the area of the tilt-wings has received a significant interest as a corresponding growing area of research and development activities, vehicles as SUAVI [6], JAXA's "AKITSU" QTWUAV [7] and QTW QUX-02 [8], quad tilt-wing UAVs where the thrust is generated by four rotors that are located on the leading edges of the four identical wings at front and rear of vehicle, the wing-rotor pairs can be tilted from vertical to horizontal position for the transition between flight modes.

Due to a change of angle of the wings and rotors, Tilt-wing UAV presents the following aerodynamic advantages: 1) Minimum drag and down wash on the wings, since the wings are always aligned with the rotor, 2) In transition flight mode, the wings will start generating lift and drag because there will be an increase in speed at the same time, and even though the lift to drag ratio is low under the transition phase, the tilt wing will still generate a fair amount of lift, meaning that the UAV will be able to utilize smaller rotors and become more efficient electric current consumption as long as it can overcome the drag [9].

Unlike tilt-rotor UAVs, the study focus of the Tilt-wing UAV is mostly the quad tilt-wing vehicle, due to its structural design similar to quadrotor. In [9] and [10] the authors present Tri tilt-wing UAVs where the thrust is generated by two main rotors and a tail rotor that pitch stabilizes, however, the focus is only with hover flight. On the other hand, the German DHL company [11], developed a dual tilt-wing UAV, where the thrust is generated only by two main rotors, nevertheless, there is no evidence of the vehicle development (structural design, control design, simulations, experimental tests, etc).

Since the thrust is generated by two rotors, the Dual tilt-wing UAV presents a great stability challenge in its three flight modes, however, the electric current consumption decreases, the vehicle's weight is smaller than the Tri or Quad tilt-wing, so the flight time increases.

In this paper a Dual Tilt-wing is presented. For VTOL flight mode, the vehicle has two main rotors that are located on the leading edges of the two wings and two ailerons that are located on the trailing edges of the wings as control surfaces. For the transition flight mode, the wings together with the rotors are tilted from 90 to 0 degrees. Finally, for horizontal flight mode it is similar to a fixed-wing, with two rotors, two ailerons, an elevator and a rudder on the empennage as control surfaces.

The main contribution of this paper is to provide the UAV's complete dynamical model, the nonlinear model is derived the Newton-Euler formulation, the model includes aerodynamic effects, as the drag and lift forces of the wings which are a function of: 1) the airstream generated by the rotors, 2) the cruise speed, 3) the tilt angle and angle of attack.

The airstream velocity generated by the rotors is studied in a test bench. Later, the projected area on the UAV wing that is affected by the airstream generated by the rotors is specified and 3D aerodynamic analysis is performed for this region.

Aerodynamic effects are included caused by the empennage. Aerodynamic coefficients of the UAV in VTOL mode are calculated by using Computational Fluid Dynamics method (CFD) and are embedded into the nonlinear dynamic model.

In investigations based on the study of tilt-wing UAVs, complete dynamic models have been developed that include wing's aerodynamic characterization or the studying the propeller effects. However, the study is only proposed in the horizontal flight mode or specific flight conditions. In [12], Benkhoud and Bouallegue considered the wing's lift and drag forces only for horizontal and transition flight modes, as function of linear velocity (V_x and V_z), tilt (γ) and attack (α) angles. Their motion equations for VTOL flight mode are similar to those of a Quadrotor. Additionally, in [13], Masuda and Uchiyama considered uncertainties such as wind in the model, and the aerodynamic coefficients were obtained by wind tunnel experiments. In [14], Cetinsoy et al. in addition to wind tunnel experiments, they performed ANSYS simulations to obtain the wing's aerodynamic coefficients. They consider that the total thrust and the desired attitude angles are functions of the wing angles, this effect are not studied for quadrotors. In [15], Garcia et al. In addition to the angle of attack, they include the sideslip angle in the mathematical model. They also accounted for the propeller effect (Propeller Momentum Theory) to obtain the aerodynamic behavior of the vehicle in horizontal flight. Other papers as [16] and [10] mention that mounting the tilt-wings does not affect a fundamental operation of the Quadrotor, likewise, the additional aerodynamic forces exerted on the body and the forces produced by the flow of air from the propellers over the wing profile are neglected.

To validate the complete dynamic model, PD controllers are designed for altitude and attitude control of the vehicle in VTOL mode, the controllers are simulated and implemented in the vehicle for real-time flight experiments.

The rest of the paper is organized as follows: Section 2 contains the Dual tilt-wing UAV complete dynamic model. In section 3 to validate the dynamic model, PD controllers are designed, simulated and implemented for altitude and attitude control of the UAV in VTOL mode. In section 4, modeling parameters are obtained. In section 5 the simulation results are analyzed. Subsequently, in section 6 the real-time flight experiments results of UAV in VTOL mode are presented. Finally, section 7 concludes the paper and future work is presented.

2 Complete Dynamic model

In this section, the UAV complete dynamic model is presented, aerodynamic effects are considered for its different flight modes. The model is obtained by employing the Euler-Newton formulation for each of its 6-degrees-of-freedom (6-DOF).

2.1 Equations of motion

Consider each element as a rigid-body in the inertial reference system, with the gravity center (cg) coincident with the aerodynamic center (ca). $E = \{x^E, y^E, z^E\}$ denotes the earth fixed inertial reference frame, $B = \{x^B, y^B, z^B\}$ denotes the body fixed reference frame with origin in the cg, $W = \{x^W, y^W, z^W\}$ denotes the mobile aerodynamic referential with origin in the ca (Figure 1).

Assuming the generalized coordinates as $Q = [q_1\ q_2]^T \in \mathbb{R}^6$, where $q_1 = [x\ y\ z]^T \in \mathbb{R}^3$ denotes the vehicle position relative at the inertial frame and $q_2 = [\phi\ \theta\ \psi]^T \in \mathbb{R}^3$ are the three Euler angles, roll, pitch and yaw respectively and represent the UAV attitude.

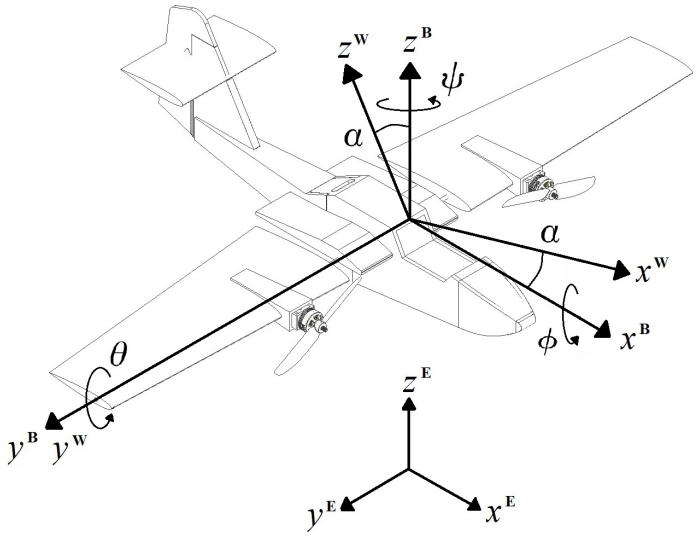

Fig. 1: UAV motion variables notation.

For transforming the axes from the body frame to the inertial frame, the rotation matrix $R^{B\to E}$ is defined, where $s* = sin\,(*)$ and $c* = cos\,(*)$.

$$R^{B\to E} = \begin{bmatrix} c\theta c\psi & c\theta s\psi & -s\theta \\ s\phi s\theta c\psi - c\phi s\psi & s\phi s\theta s\psi + c\phi c\psi & s\phi c\theta \\ c\phi s\theta c\psi + s\phi s\psi & c\phi s\theta s\psi - s\phi c\psi & c\phi c\theta \end{bmatrix} \tag{1}$$

For transforming the axes from the mobile aerodynamic referential to body frame, the rotation matrix $R^{W\to B}$ is defined, where α is the rotation angle (angle of attack) of the tilt mechanism of wing and rotor [17,18].

$$R^{W\to B} = \begin{bmatrix} c\alpha & 0 & -s\alpha \\ 0 & 1 & 0 \\ s\alpha & 0 & c\alpha \end{bmatrix} \tag{2}$$

Therefore, the UAV complete dynamic model is obtained, where the translational motion is based to Newton's second law with respect to inertial reference frame and the rotational motion with Euler's law with respect to body fixed reference frame [19].

$$\bar{m}\dot{v}^E = R^{B\to E}F^B + mG^I \tag{3}$$

$$I\dot{\Omega} + \Omega \times I\Omega = \Gamma^B \tag{4}$$

where $F^B \in \mathbb{R}^3$ and $\Gamma^B \in \mathbb{R}^3$ are the forces and moments acting on the vehicle, $\bar{m} = diag\,(m) \in \mathbb{R}^{3\times3}$ is the UAV mass, $\dot{v}^E = \ddot{q}_1 = [\ddot{x}\ \ddot{y}\ \ddot{z}]^T \in \mathbb{R}^3$ denotes the linear acceleration, $\Omega = R\dot{q}_2 = [p\ q\ r]^T \in \mathbb{R}^3$ describes the angular velocity and $\dot{\Omega} = R\ddot{q}_2 \in \mathbb{R}^3$ the angular acceleration according to the Euler angles, with $\dot{q}_2 = \left[\dot{\phi}\ \dot{\theta}\ \dot{\psi}\right]^T \in \mathbb{R}^3$, $\ddot{q}_2 = \left[\ddot{\phi}\ \ddot{\theta}\ \ddot{\psi}\right]^T \in \mathbb{R}^3$ and the rotation matrix R defined as:

$$R = \begin{bmatrix} c\theta c\psi & s\psi & 0 \\ -c\theta s\psi & c\psi & 0 \\ s\theta & 0 & 1 \end{bmatrix} \tag{5}$$

Furthermore, $I \in \mathbb{R}^{3\times3}$ describes the inertia tensor matrix, whose value depends on the body mass distribution, if the body symmetry on the $x^B - z^B$ plane is considered and the remaining inertia products are low compared to the main moments, the inertia tensor is approximated by:

$$I = \begin{bmatrix} I_x & 0 & 0 \\ 0 & I_y & 0 \\ 0 & 0 & I_z \end{bmatrix} \tag{6}$$

2.1.1 Translational dynamic

From equations (1) and (3), the UAV translational motion may be re-written as:

$$\begin{aligned} m\ddot{x} &= F_x^B(c\theta c\psi) + F_y^B(c\theta s\psi) - F_z^B(s\theta) \\ m\ddot{y} &= F_x^B(s\phi s\theta c\psi - c\phi s\psi) + F_y^B(s\phi s\theta s\psi + c\phi c\psi) + F_z^B(s\phi c\theta) \\ m\ddot{z} &= F_x^B(c\phi s\theta c\psi + s\phi s\psi) + F_y^B(c\phi s\theta s\psi - s\phi c\psi) + F_z^B(c\phi c\theta) - mg \end{aligned} \tag{7}$$

The total forces (F^B) acting on the vehicle is the sum of the rotors forces (F_R^B) and the aerodynamic loads (F_W^B), $F^B = \left[F_x^B\ F_y^B\ F_z^B\right]^T = \left[R^{W\to B}F_R^B + R^{W\to B}F_W^B\right]$.

The vehicle consists of two rotors generating the lift force for vertical flight mode and a thrust force for horizontal flight mode. With a fuselage that for now, its aerodynamic effect is neglected, two wings and an empennage that generate aerodynamic forces as function of the angle of attack, the control surfaces (ailerons, elevator and rudder), relative wind velocity and airstream generated by the rotors.

$$\begin{aligned} F_x^B &= c\alpha\,(F_{R1} + F_{R2}) - c\alpha\,(D_{W1} + D_{W2} + D_{We} + D_{Wr}) \\ &\quad -s\alpha\,(L_{W1} + L_{W2} + L_{We}) \\ F_y^B &= L_{Wr} \\ F_z^B &= s\alpha\,(F_{R1} + F_{R2}) - s\alpha\,(D_{W1} + D_{W2} + D_{We} + D_{Wr}) \\ &\quad +c\alpha\,(L_{W1} + L_{W2} + L_{We}) \end{aligned} \tag{8}$$

where L is the aerodynamic lift and D is the aerodynamic drag of the wings (W), the horizontal stabilizer (We) and the vertical stabilizer (Wr), (Figure 2).

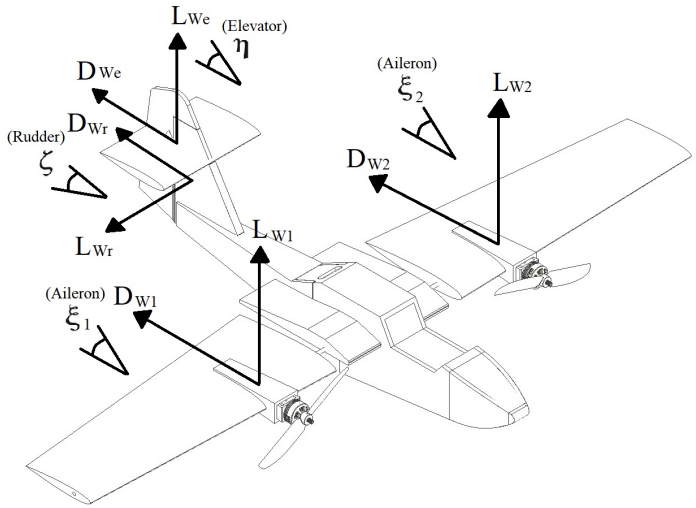

Fig. 2: Aerodynamic forces and controls notation.

2.1.2 Rotational dynamic

From equations (4), (5) and (6), the UAV rotational motion may be re-written as:

$$\begin{aligned}
\ddot{\phi} &= \tfrac{1}{c\theta c\psi}\left[-\ddot{\theta}s\psi + \dot{\phi}\dot{\theta}s\theta c\psi + \dot{\phi}\dot{\psi}c\theta s\psi - \dot{\theta}\dot{\psi}c\psi + \tfrac{1}{I_x}\left(\Gamma_x^B - \left(-\dot{\phi}c\theta s\psi + \dot{\theta}c\psi\right)\left(\dot{\phi}s\theta + \dot{\psi}\right)(I_y - I_z)\right)\right] \\
\ddot{\theta} &= \tfrac{1}{c\psi}\left[\ddot{\phi}c\theta s\psi - \dot{\phi}\dot{\theta}s\theta s\psi + \dot{\phi}\dot{\psi}c\theta c\psi + \dot{\theta}\dot{\psi}s\psi + \tfrac{1}{I_y}\left(\Gamma_y^B - \left(\dot{\phi}c\theta c\psi + \dot{\theta}s\psi\right)\left(\dot{\phi}s\theta + \dot{\psi}\right)(I_z - I_x)\right)\right] \\
\ddot{\psi} &= -\ddot{\phi}s\theta - \dot{\phi}\dot{\theta}c\theta + \tfrac{1}{I_z}\left(\Gamma_z^B - \left(\dot{\phi}c\theta c\psi + \dot{\theta}s\psi\right)\left(-\dot{\phi}c\theta s\psi + \dot{\theta}c\psi\right)(I_x - I_y)\right)
\end{aligned} \tag{9}$$

The total moments (Γ^B) acting on the vehicle is the sum of the main moments provided by the control surfaces (Γ_c^B), the gyroscopic moment generated by the variation of the propeller rotation axis (Γ_g^B), and the drag moment (Γ_D^B) due to the propeller drag force, $\Gamma^B = \left[\Gamma_x^B\ \Gamma_y^B\ \Gamma_z^B\right]^T = \left[\Gamma_c^B + \Gamma_g^B + \Gamma_D^B\right]$.

With Y_R, Y_W, X_e, X_r, Z_e as the distances of the forces acting on the vehicle of the rotors, wings, horizontal and vertical stabilizer respectively (Figure 3), the main moments are defined as follow:

$$\Gamma_c^B = \begin{bmatrix} s\alpha\left(Y_{R1}F_{R1} - Y_{R2}F_{R2}\right) + c\alpha\left(Y_{W1}L_{W1} - Y_{W2}L_{W2}\right) - s\alpha\left(Y_{W1}D_{W1} - Y_{W2}D_{W2}\right) \\ -Z_e\left(c\alpha D_{We} + s\alpha L_{We}\right) + X_e\left(-s\alpha D_{We} + c\alpha L_{We}\right) - X_r\left(s\alpha D_{Wr}\right) \\ c\alpha\left(Y_{R2}F_{R2} - Y_{R1}F_{R1}\right) + s\alpha\left(Y_{W1}L_{W1} - Y_{W2}L_{W2}\right) + c\alpha\left(Y_{W1}D_{W1} - Y_{W2}D_{W2}\right) - X_rL_{Wr} \end{bmatrix} \tag{10}$$

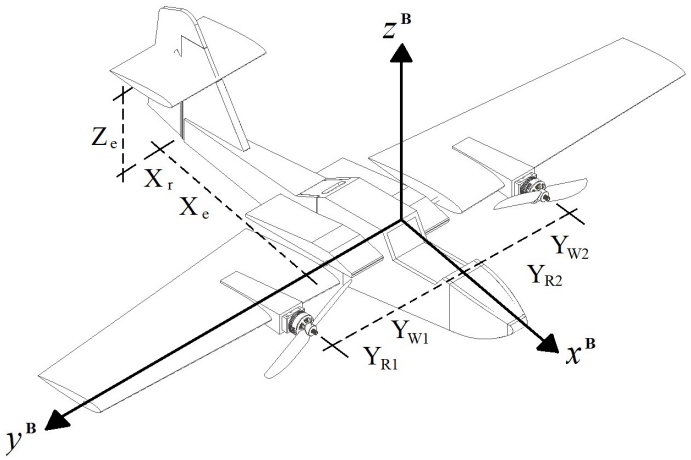

Fig. 3: Distances of the forces acting on the UAV.

The gyroscopic moment, with I_{zr} as the propeller inertia moment on its rotation axis and ω_R as the rotor angular velocity, is described as:

$$\Gamma_g^B = \begin{bmatrix} s\alpha I_{zr} q\left(\omega_{R2} - \omega_{R1}\right) \\ c\alpha I_{zr} r\left(\omega_{R2} - \omega_{R1}\right) + s\alpha I_{zr} p\left(\omega_{R1} - \omega_{R2}\right) \\ c\alpha I_{zr} q\left(\omega_{R1} - \omega_{R2}\right) \end{bmatrix} \tag{11}$$

Finally, the drag moment, where D_R is the propeller drag force, is defined as:

$$\Gamma_D^B = \begin{bmatrix} s\alpha\left(Y_{R2} D_{R2} - Y_{R1} D_{R1}\right) \\ 0 \\ c\alpha\left(Y_{R1} D_{R1} - Y_{R2} D_{R2}\right) \end{bmatrix} \tag{12}$$

3 Mathematical model validation

In this section, the complete mathematical model is validated. For simplicity, the UAV's different flight dynamics are studied separately. First, the flight in VTOL mode is analyzed, therefore, the equations are simplified for VTOL flight mode conditions, subsequently PD controllers are designed for altitude and attitude control.

Assumptions

A) The rotors and wings are in vertical position, so that the angle $\alpha = 90°$, therefore, $cos(\alpha)= 0$ y $sin(\alpha)= 1$.
B) The x and y displacements are neglected for are small compared to the z displacement (Altitude).
C) The wings and horizontal stabilizer do not generate lift forces in function of the angle of attack (α), only in function of the control surfaces (only ailerons).
D) The vertical stabilizer does not generate aerodynamic effects.

E) Since gyroscopic effects on propellers are small enough, they are neglected.
F) The yaw (ψ) and roll (ϕ) motions are small compared to pitch (θ), so that $sin(A) = A$ and $cos(A) = 1$.

From equations (7) and (9), the resulting linearized altitude and attitude dynamics can be expressed in earth fixed inertial reference frame, as:

$$\begin{aligned}
&m\ddot{z} = (u_1 - D_{W1} - D_{W2} - D_{We})(c\theta) - mg \\
&\ddot{\phi} = \tfrac{1}{c\theta}\left[-\ddot{\theta}\psi + \dot{\phi}\dot{\theta}s\theta + \dot{\phi}\dot{\psi}c\theta\psi - \dot{\theta}\dot{\psi} - \tfrac{1}{I_x}\left(\left(-\dot{\phi}c\theta\psi + \dot{\theta}\right)\left(\dot{\phi}s\theta + \dot{\psi}\right)(I_y - I_z)\right) + \tfrac{1}{I_x}(u_2 - Y_{W1}D_{W1} - Y_{W2}D_{W2})\right] \\
&\ddot{\theta} = \ddot{\phi}c\theta\psi - \dot{\phi}\dot{\theta}s\theta\psi + \dot{\phi}\dot{\psi}c\theta + \dot{\theta}\dot{\psi}\psi - \tfrac{1}{I_y}\left(\left(\dot{\phi}c\theta + \dot{\theta}\psi\right)\left(\dot{\phi}s\theta + \dot{\psi}\right)(I_z - I_x)\right) + \tfrac{1}{I_y}(u_3 - X_e D_{We}) \\
&\ddot{\psi} = -\ddot{\phi}s\theta - \dot{\phi}\dot{\theta}c\theta - \tfrac{1}{I_z}\left(\left(\dot{\phi}c\theta + \dot{\theta}\psi\right)\left(-\dot{\phi}c\theta\psi + \dot{\theta}\right)(I_x - I_y)\right) + \tfrac{1}{I_z}(u_4)
\end{aligned} \tag{13}$$

where, u_1 is a virtual control input in terms of actuating forces and u_2, u_3 and u_4 are a virtual control inputs in terms of actuating torques.

$$\begin{aligned}
u_1 &= F_{R1} + F_{R2} \\
u_2 &= Y_{R1}F_{R1} - Y_{R2}F_{R2} \\
u_3 &= -Z_e L_{We} \\
u_4 &= Y_{W1}L_{W1} - Y_{W2}L_{W2}
\end{aligned} \tag{14}$$

A PD controller [20] is designed for altitude control and three PD controllers are designed for attitude control. Controllers designed are defined by the following equations:

$$\begin{aligned}
u_z &= k_{p,z}e_z + k_{d,z}\dot{e_z} + k_{i,z}\int e_z \\
u_\phi &= k_{p,\phi}e_\phi + k_{d,\phi}\dot{e_\phi} + k_{i,\phi}\int e_\phi \\
u_\theta &= k_{p,\theta}e_\theta + k_{d,\theta}\dot{e_\theta} + k_{i,\theta}\int e_\theta \\
u_\psi &= k_{p,\psi}e_\psi + k_{d,\psi}\dot{e_\psi} + k_{i,\psi}\int e_\psi
\end{aligned} \tag{15}$$

4 Model parameters of the vehicle

This section is focused in obtaining the UAV's physical parameters to be used for the simulation of the designed altitude and attitude controllers.

4.1 Vehicle mass

Because the vehicle's thrust is generated by two rotors for vertical flight mode, the vehicle has to be lightweight and capable of withstanding the possible loadings in its different flight modes. Therefore, for the UAV construction, foam board is used for the fuselage, boom and landing gear, EPS for wings and vertical and horizontal stabilizer, with carbon fiber tubes in the wings as reinforcements. By the vehicle structure, electronic system, rotors and Li-Po battery, the vehicle total weight is 1 Kg.

4.2 Inertia tensor

A Computer Aided Design (CAD) software is used to obtain the inertia tensor. First, the vehicle is designed, after, the proper material type is added to the different parts in the model so that the weight, mass center, and inertia tensor matrix could be estimated, as showed in (Figure 4).

So that the mass center is coincident with the aerodynamic center, both are positioned at 25 % of the symmetrical profile's chord of wing.

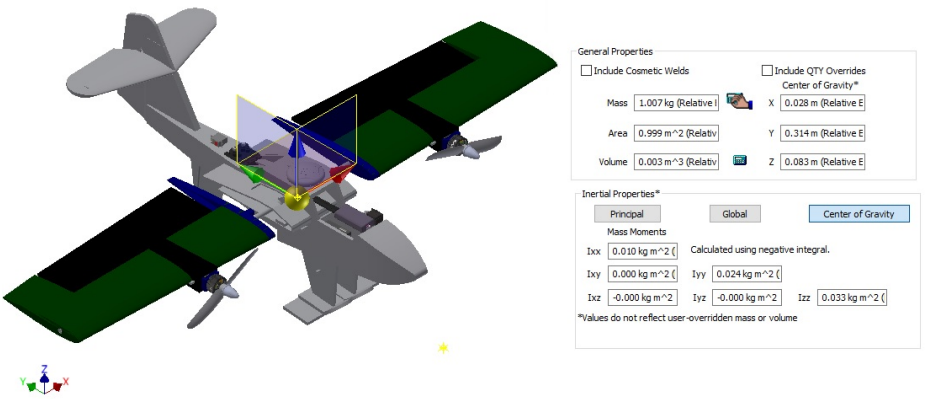

Fig. 4: UAV inertia tensor.

4.3 Aerodynamic effects

During vertical flight, the wings and horizontal stabilizer generate aerodynamic effects that are included into the dynamic model.

A symmetrical airfoil (NACA 0012) is considered for the wing, where the airstream generated by the rotors is aligned with the wing chord line, thus the lift force and moment is canceled due to the symmetrical flow condition. Therefore, only the drag force is considered.

For the drag force calculation, the wing can be divided into two areas due to aerodynamic interference, an area that is affected by airstream generated by the rotors and an area that is affected by the vehicle's rate of climb in vertical flight mode (Figure 5).

Firstly, the projected area on the wing that is affected by the airstream generated by the rotors is specified. The maximum velocity airstream generated by the rotors is obtained in a test bench (Figure 6a). Propeller 10" x 4.5" is used for the propulsion force. (Figure 6b) show the velocity airstream is function of rotor's throttle and (Figure 6c) show the throttle in function of rotor's propulsion force.

With the maximum velocity airstream generated by the rotors obtained, 3D aerodynamic analysis is performed for this region. The UAV's drag coefficient (C_D) is calculated by using

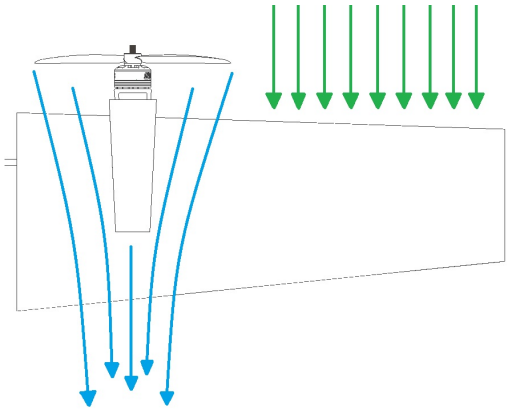

Fig. 5: Area affected by the rate of climb and area affected by the airstream generated by the rotors.

Computational Fluid Dynamics method (CFD). The drag force [21,22] is obtained by the following expression:

$$D = \tfrac{1}{2}\rho V^2 S C_D \tag{16}$$

where, ρ is the air density, S the wing planform area, V the airflow velocity, C_D the drag coefficient. Finally, the drag force is assumed as a polynomial function in terms of rotor's propulsion force.

The drag force of wing's second section and horizontal stabilizer are a function of the rate of climb in vertical flight mode. Similarly, the drag coefficients are calculated by using CFD method and the drag forces by the equation (16). A polynomial function in terms of the rate of climb for the wing's drag force and the horizontal stabilizer is obtained.

5 Simulation results

Numerical simulations validate the proposed complete dynamic model with aerodynamic effects considered and PD controllers designed. The simulations are carried out in Matlab/Simulink environment.

Table 1 shows the operation range of UAV's actuators. In Table 2 the parameters and the applicable dimensions to the vehicle are shown. Conditions of the simulation are shown in Table 3. Last, the control parameters utilized are shown in Table 4.

Table 1: Operation range of actuators.

Parameter	Value	Unit
Propeller thrust	$0 \leq F_{Rn} \leq 10$ (n=1,2)	N
Aileron angle	$-\pi/6 \leq \xi_n \leq \pi/6$ (n=1,2)	rad
Tilt angle	$\alpha_n = \pi/2$ (n=1,2)	rad

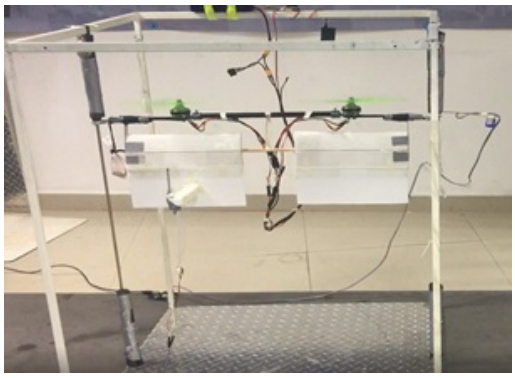

(a) Test bench to studied the airstream generated by the rotors.

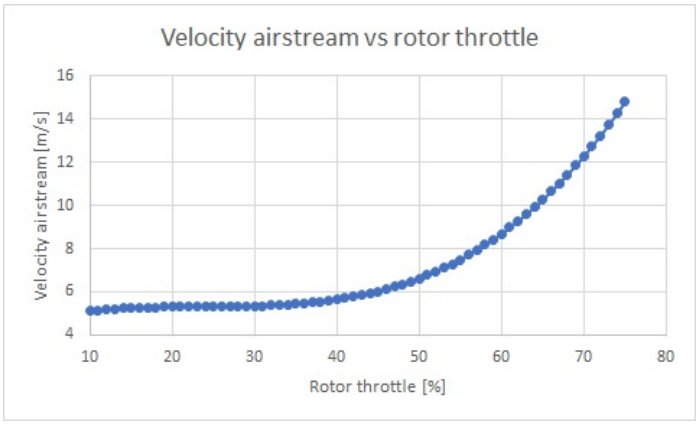

(b) Velocity airstream vs rotor throttle.

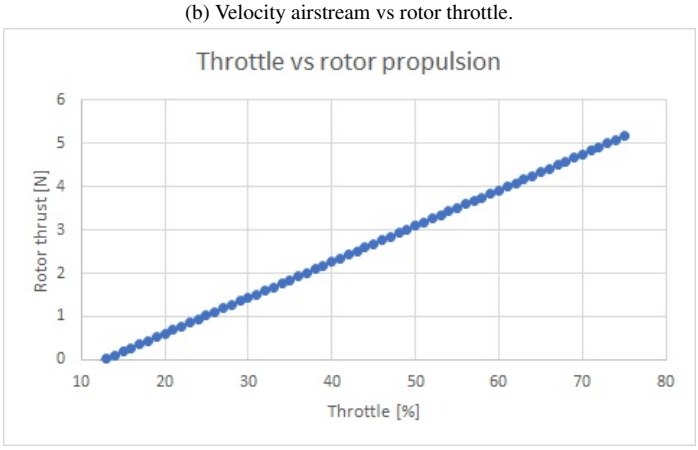

(c) Throttle vs rotor propulsion.

Fig. 6: Aerodynamic effects of the area on the wing that is affected by the airstream generated by the rotors

Table 2: Parameters.

Parameter	Value	Unit
m	1	kg
g	9.80665	m/s^2
I_x	0.024	Kg $\cdot$ m^2
I_y	0.010	Kg $\cdot$ m^2
I_z	0.033	Kg $\cdot$ m^2
Y_{w1}	0.25	m
Y_{w2}	0.25	m
ρ	1.225	Kg/m^3
S	0.08	m^2

Table 3: Simulation conditions.

Parameter		Value		Unit
Velocity initial	V_o	$\begin{bmatrix}0 & 0 & 0\end{bmatrix}^T$		m/s
Angular velocity initial	Ω_o	$\begin{bmatrix}0 & 0 & 0\end{bmatrix}^T$		rad/s
Attitude initial	q_2	$\begin{bmatrix}0 & 0 & 0\end{bmatrix}^T$		rad
Target position	z_d	$\begin{bmatrix}0 & 0 & 10\end{bmatrix}^T$	(Time $\leq$ 3 s)	m
	ϕ_d	$\begin{bmatrix}\pi/10 & 0 & 0\end{bmatrix}^T$	(Time = 5 s)	rad
	θ_d	$\begin{bmatrix}0 & \pi/10 & 0\end{bmatrix}^T$	(Time = 8 s)	rad
	ψ_d	$\begin{bmatrix}0 & 0 & \pi/10\end{bmatrix}^T$	(Time = 10 s)	rad

Table 4: Control parameters.

K	Roll	Pitch	Yaw	Altitude
k_p	0.21	0.21	0.4	100
k_d	0.055	0.105	0.09	20

A vertical take-off, hover and landing scenario is considered. During the first 3 seconds, the vehicle takes off and climbs to 10 m. Then, at 5 seconds, the vehicle rotates on the X axis (Roll) to 15 degrees, later, at 8 seconds, the vehicle rotates on the Y axis (Pitch) to 15 degrees and at 10 seconds, the vehicle rotates on the Z axis (Yaw) to 15 degrees, preserving its altitude. Finally, the vehicle lands in 20 seconds.

Figure 7 shows the corresponding control signals to the motors (rotors) and servomotors (ailerons). Notice that during vertical take-off, each rotor generates approximately 5N at 60% throttle that compensate the vehicle's weight and the drag forces of the wing and horizontal stabilizer. When the vehicle carries out a rotation motion (Roll, pitch, yaw), vertical component of thrust decreases, therefore, rotors thrust increase without exceeding its maximum capacity to preserving its altitude.

Also, notice that the UAV reached the desired altitude (Figure 8) while the error signals (Figure 9) rapid converge to the reference signal, without intense overshots and oscillations despite using PD controllers. Even, after performing the roll (Figure 10), pitch (Figure 11) and Yaw (Figure 12) motions, is managed to perform a quick recovery of the system stability in only a seconds.

Figure 13 shows the effects drag forces of the wings and horizontal stabilizer that in the model are included.

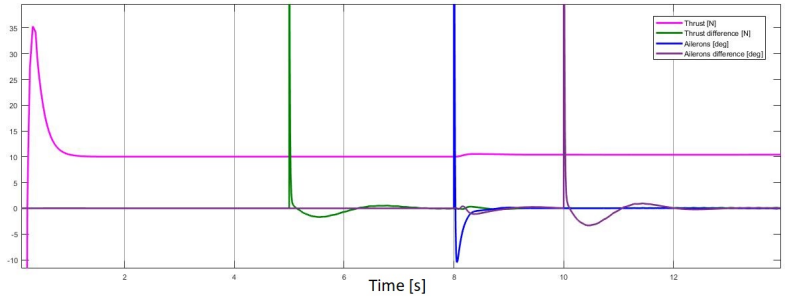

Fig. 7: Responses of control inputs.

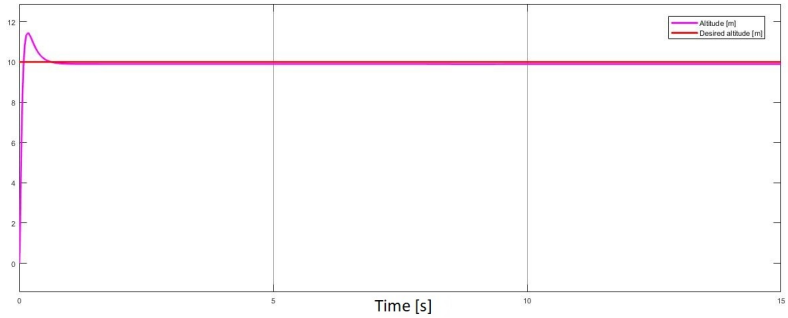

Fig. 8: Altitude control response.

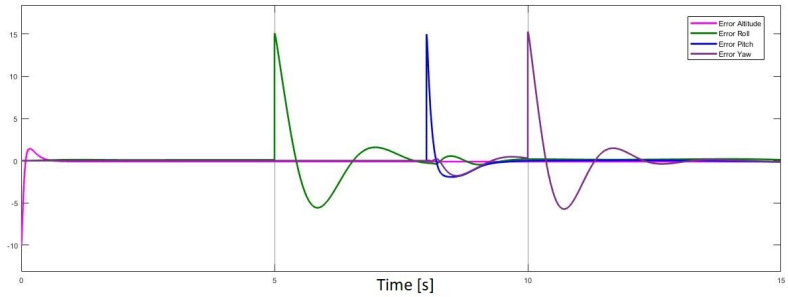

Fig. 9: Error signals.

6 Flight test results in real-time

This section shows the real-time results of the vehicle's flight tests to perform for vertical take-off, hover and landing. The tests start with a vertical take-off, hover flight at desired altitude, after, rotation motions (roll, pitch and yaw), and finally, a vertical landing.

Figure 14a show is the altitude's response, where results similar to the numerical simulation are obtained. Figures 14b, 14c and 14d shows the real-time responses of the vehicle orientation, roll, pitch and yaw, respectively. A stable flight hover is accomplished which

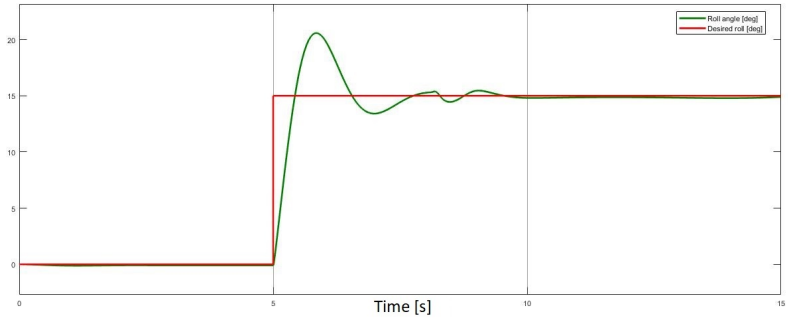

Fig. 10: Roll angle and control.

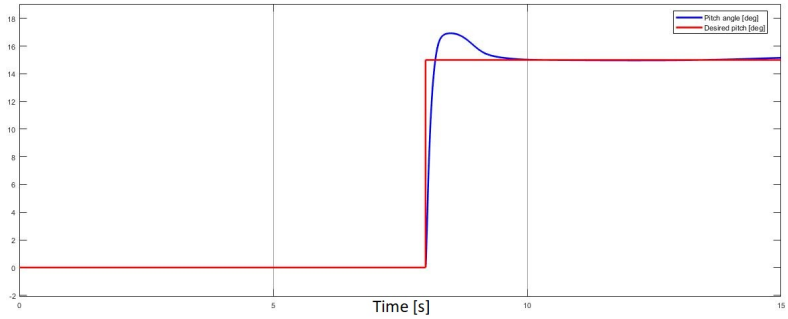

Fig. 11: Pitch angle and control.

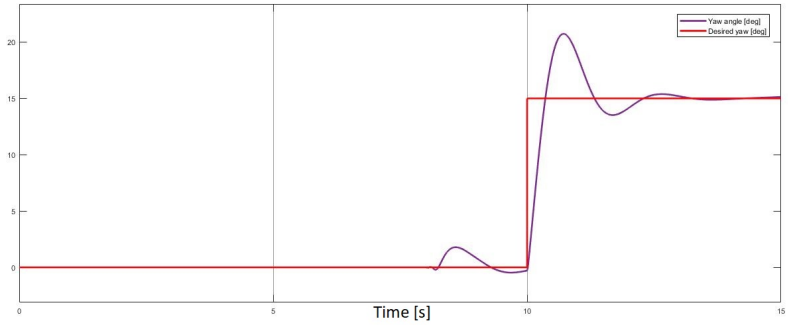

Fig. 12: Yaw angle and control.

the control inputs, rotors and ailerons, never exceeded its constraints, despite the vehicle is drifted by side wind impact on the wings in vertical position.

The roll angle did not exceeded its reference for more than 4 degrees, whereas the error in yaw reference tracking is bounded at 10 degrees. The pitch reference is kept at 8 degrees, although, this reference is more difficult to stabilize.

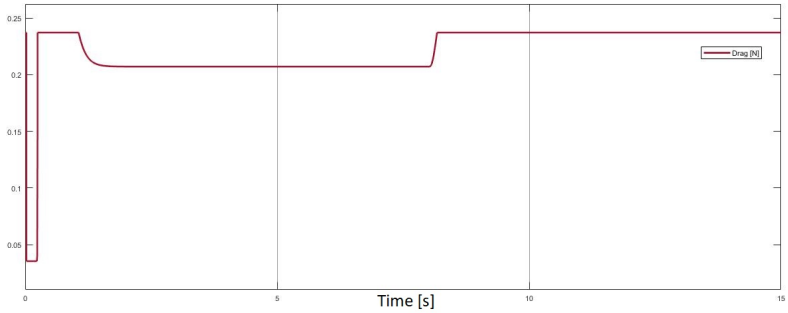

Fig. 13: Aerodynamic drag force.

(a) Altitude real-time.

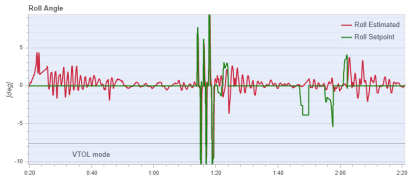

(b) Roll real-time.

(c) Pitch real-time.

(d) Yaw real-time.

Fig. 14: Flight test results in real-time

7 Conclusions and future work

In this paper, a Dual Tilt-wing is studied. The UAV complete dynamic model is obtained using the Newton-Euler formulation, aerodynamic effects are included of the wing and empennage as function of the cruise speed, tilt angle and angle of attack. For aerodynamic analysis, the wing is divided into two sections, an area that is affected by airstream generated by the rotors and an area that is affected by cruising speed. Experiments in a test bench and 3D simulations are performed to obtain the aerodynamic effects that are embedded to the model.

To validate the UAV dynamic model, PD controllers are designed for altitude and attitude control of the vehicle in vertical flight mode. Numerical simulations and flight tests in real-time showed that the error signals rapidly converge to the reference signals, accomplished stable flights in vertical mode.

As future work, the side wind effect on the wings in vertical flight mode will be included in the dynamic model, the model will be validated for the transition and horizontal flight

modes, so that the three flight modes of the Dual Tilt-wing UAV can be studied with control approaches to improve the stability of the controlled system.

References

1. K. Nonami, F. Kendoul, S. Suzuki, W. Wang and D. Nakazawa, *Autonomous Flying Robots: Unmanned Aerial Vehicles and Micro Aerial Vehicles*, Springer, London (2010).
2. B. Yuksek, A. Vuruskan, U. Ozdemir, M. A. Yukselen and G. Inalhan, *Transition Flight Modeling of a Fixed-Wing VTOL UAV*, Journal of Intelligent & Robotic Systems, Vol.84, pp.83-105 (2016)
3. G. Flores, J. Escareo, R. Lozano and S. Salazar, *Quad-Tilting Rotor Convertible MAV: Modeling and Real-Time Hover Flight Control*, Journal of Intelligent & Robotic Systems, Vol.65, pp.457-471 (2012)
4. C. Chen, J. Zhang, D. Zhang and L. Shen, *Control and flight test of a tilt-rotor unmanned aerial vehicle*, International Journal of Advanced Robotic Systemss, pp.1-12 (2017), doi:10.1177/1729881416678141
5. Y. O. Aktas, U. Ozdemir, Y. Dereli, A. F. Tarhan, A. Cetin, A. Vuruskan, B. Yuksek, H. Cengiz, S. Basdemir, M. Ucar, M. Genctav, A. Yukselen, I. Ozkol, M. O. Kaya and G. Inalhan, *Rapid prototyping of a Fixed-Wing VTOL UAV for Design Testing*, Journal of Intelligent & Robotic Systems, Vol.84, pp.639-664 (2016)
6. E. Centinsoy, E. Sirimoglu, K. T. Oner, C. Hancer, M. Unel, M. F. Aksit, I. Kandemir and K. Gulez, *Design and development of a tilt-wing UAV*, Turkish Journal of Electrical Engineering and Computer Sciences, Vol.19, No.5, pp.733-741 (2011)
7. M. Sato and K. Muraoka, *Flight Controller Design and Demonstration of Quad-Tilt-Wing Unmanned Aerial Vehicle*, Journal of Guidance, Control and Dynamics, Vol.38, No.6, pp.1-12 (2015)
8. K. Muraoka, N. Okada and D. Kubo, *Quad Tilt Wing VTOL UAV: Aerodynamic Characteristics and Prototype Flight Test*, AIAA Infotech@Aerospace Conference (2009), doi: 10.2514/6.2009-1834
9. A. Lindqvist, E. Fresk and G. Nikolakopoulos, *Optimal Design and Modeling of a Tilt Wing Aircraft*, 23rd Mediterranean Conference on Control and Automation (2015), doi: 10.1109/MED.2015.7158828
10. E. Small, E. Fresk, G. Andrikopoulos and G. Nikolakopoulos, *Modelling and Control of a Tilt-Wing Unmanned Aerial Vehicle*, 24th Mediterranean Conference on Control and Automation (2016), doi: 10.1109/MED.2016.7536050
11. *DHL Parcelcopter 3.0*, `https://www.dpdhl.com/en/media-relations/specials/dhl-parcelcopter.html`
12. K. Benkhoud and S. Bouallegue, *Dynamics modeling and advanced metaheuristics based LQG controller design for a Quad Tilt Wing UAV*, International Journal of Dynamics and Control, Vol.6, No.2, pp.630-651 (2018)
13. K. Masuda and K. Uchiyama, *Robust control design for Quad Tilt-wing UAV*, Aerospace (2018), Vol.5, No.1, doi:10.3390/aerospace5010017
14. E. Cetinsoy, S. Dikyar, C. Hancer, K. T. Oner, E. Sirimoglu, M. Unel and M. F. Aksit, *Design and construction of a novel quad tilt-wing UAV*, Mechatronics, Vol.22, No.6, pp.723-745 (2012)
15. O. Garcia, P. Castillo, K. C. Wong and R. Lozano, *Attitude stabilization with real-time experiments of a tail-sitter aircraft in horizontal flight*, Journal of Intelligent & Robotic Systems, Vol.65, No.1-4, pp.123-136 (2012)
16. R. Takeuchi, K. Watanabe and I. Nagai, *Development and control of tilt-wings for a tilt-type Quadrotor*, IEEE International Conference on Mechatronics and Automation (2017), doi: 10.1109/ICMA.2017.8015868
17. B. Etkin and L. D. Reid, *Dynamics of flight: stability and control*, 3rd edition, John Wiley & Sons, Inc. USA (1996)
18. M. V. Cook, *Flight dynamics principles: A linear systems approach to aircraft stability and control*, 3rd edition, Elsevier Ltd. USA (2013)
19. J. Escareño, S. Salazar and R. Lozano, *Modelling and control of a convertible VTOL aircraft*, IEEE Conference on Decision & Control, San Diego, CA (2006)
20. K. T. Oner, E. Cetinsoy, E. Sirimoglu, C. Hancer, M. Unel, M. F. Aksit, K. Gulez and I. Kandemir, *Mathematical modeling and vertical flight control of a tilt-wing UAV*, Turkish Journal of Electrical Engineering and Computer Sciences, Vol.20, No.1 (2012), doi: 10.3906/elk-1007-624
21. I. H. Abbott and A. E. Von Doenhoff, *Theory of wing sections*, Dover Publications, Inc. New York (1959)
22. J. D. Anderson, Jr, *Fundamentals of Aerodynamics*, 5th edition, McGraw-Hill, New York (2011)